^{1}H NMR Investigation of the Electronic and Molecular Structure of the Four-Iron Cluster Ferredoxin from the Hyperthermophile *Pyrococcus furiosus*. Identification of Asp 14 as a Cluster Ligand in Each of the Four Redox States†

Luigi Calzolai,‡,§ Carol M. Gorst,‡ Zhi-Hao Zhao,|| Quincy Teng,‡,⊥ Michael W. W. Adams,|| and Gerd N. La Mar*,‡

Department of Chemistry, University of California, Davis, California 95616, and Department of Biochemistry and Molecular Biology and Center for Metalloenzyme Studies, University of Georgia, Athens, Georgia 30602

Received May 9, 1995; Revised Manuscript Received June 26, 1995®

ABSTRACT: The molecular and electronic structure of the four-iron cluster of the ferredoxin (Fd) from the hyperthermophilic archaeon, *Pyrococcus furiosus*, *Pf* (which has only three Cys in the cluster binding consensus sequence), has been investigated by ^{1}H NMR in order to determine the identity of the non-cysteinyl cluster ligand in each of the four redox states [Gorst, C. M., Zhou, Z. H., Ma, K., Teng, Q., Howard, J. B., Adams, M. W., & La Mar, G. N. (1995) *Biochemistry 34*, 8788−8795], and to characterize the electron spin ground state for the reduced cluster which at 10 K exhibits an unusual predominant $S = {}^3/_2$ ground state [Conover, R. C., Kowal, A. T., Fu, W., Park, J.-B., Aono, S., Adams, M. W. W., & Johnson, M. K. (1990) *J. Biol. Chem. 265*, 8533−8541]. It is demonstrated that a combination of 1D and 2D NMR tailored to relaxed resonances allows the location of four hyperfine shifted and paramagnetically relaxed spin systems which dictates that all four cluster ligands are amino acid side chains, rather than a solvent water/hydroxide at the unique non-Cys ligation site. Three of the ligands could be sequence-specifically assigned to the three Cys residues (positions 11, 17, and 56) in the consensus sequence for cluster binding, hence identifying the fourth ligand as Asp 14. It is concluded that the identification of Asp ligation to a 4Fe cluster is readily achieved in the reduced, but not in the oxidized cluster of Fd. Analysis of the relaxation properties and pattern of the hyperfine shifts in *Pf* Fd reveals very strong similarities to other Fds with $S = {}^1/2$ ground states, leading to the conclusion that the $S = {}^3/_2$ ground state is not detected in solution at ambient temperatures, and this is independent of the redox state of the two remaining Cys residues in the protein (positions 21 and 48). However, the electron self-exchange rate for 4Fe *Pf* Fd is significantly slower than for other 4Fe Fd with complete Cys ligation. Changes in the pattern of hyperfine shifts between oxidized and reduced clusters for the four ligands in *Pf* Fd reveal that the most significant variation occurs for the Asp 14 orientation, suggesting that the altered Asp orientation may "gate" the electron transfer.

The cubane-type iron sulfur clusters (Figure 1) occur in numerous small electron transfer proteins, the ferredoxins (Fds),[1] $[Fe_4S_4]^{+1,+2}$ and/or $[Fe_3S_4]^{0,+1}$, and high potential iron sulfur proteins (Hipips), $[Fe_4S_4]^{+2,+3}$. They are also found in a wide variety of enzymes in which they typically, although not always, play an electron transfer role (for reviews, see Cammack et al., 1977; Howard & Rees, 1991; Beinert, 1990; Cammack, 1992; Matsubara & Saeki, 1992; Johnson, 1994; Moura et al., 1994). The cluster ligands in Fds and Hipip are invariably four Cys residues that occur in consensus sequences characteristic for each type of electron transfer protein. In the majority of the bacterial type Fd, the protein possesses two consensus sequences for two clusters which are related by a pseudo-twofold symmetry.

In contrast to Fds, enzymes which have a cubane-type iron sulfur cluster that participates in catalysis rather than in electron transfer, the cluster may be functionalized by non-cysteinyl ligation. The prototypical example is aconitase, in which the unique Fe site of its 4Fe cluster has a solvent hydroxyl as a fourth ligand in the absence of substrate, while substrate binding results in a six-coordinate Fe site with two ligands from the substrate carboxylate (Beinert & Kennedy, 1989; Kennedy & Stout, 1992; Lauble et al., 1994). Aconitase is representative of a large class of hydratase-type enzymes that contain a [4Fe-4S] cluster, a class which includes serine dehydratase, fumarase, and isopropyl malate isomerase (Emptage, 1988). Such enzymes are typically purified aerobically in an inactive 3Fe form, and reconstitution of the cluster with Fe^{2+} to the 4Fe form is required to restore activity (Flint et al., 1993; Hofmeister et al., 1994). Such properties are strongly indicative of incomplete cysteinyl coordination to the functional 4Fe cluster. However,

† This research is supported by grants from the National Science Foundation [DMB 91-04180 (G.N.L.) and MCB 94-05783 (M.W.W.A.)] and the National Institutes of Health [GM 45597 (M.W.W.A.)].

* Address correspondence to this author at the Department of Chemistry, University of California, Davis, CA 95616. Phone: (916) 752-0958; FAX: (916) 752-8995; e-mail: lamar@indigo.ucdavis.edu.

‡ University of California, Davis.

§ Present address: Department of Chemistry, University of Siena, Siena, Italy.

|| University of Georgia.

⊥ Present address: Department of Chemistry, University of Georgia, Athens, GA 30602.

® Abstract published in *Advance ACS Abstracts,* August 15, 1995.

[1] Abbreviations: Fd, ferredoxin; Hipip, high potential iron sulfur protein; *Pf*, *Pyrococcus furiosus*; *Tl*, *Thermococcus litoralis*; *Cp*, *Clostridium pasteurianum*; *Ca*, *Clostridium acidi urici*; *Dg*, *Desulfovibrio gigas*; *Da*, *Desulfovibrio africanus*; NOE, nuclear Overhauser effect; NOESY, 2D nuclear Overhauser effect spectroscopy; MCOSY, magnitude correlation NMR spectroscopy; TOCSY, total correlation spectroscopy; DSS, 2,2-dimethyl-2-silapentane-5-sulfonate; ppm, parts per million; NMR, nuclear magnetic resonance; WEFT, water-eliminated Fourier transformation.

0006-2960/95/0434-11373$09.00/0

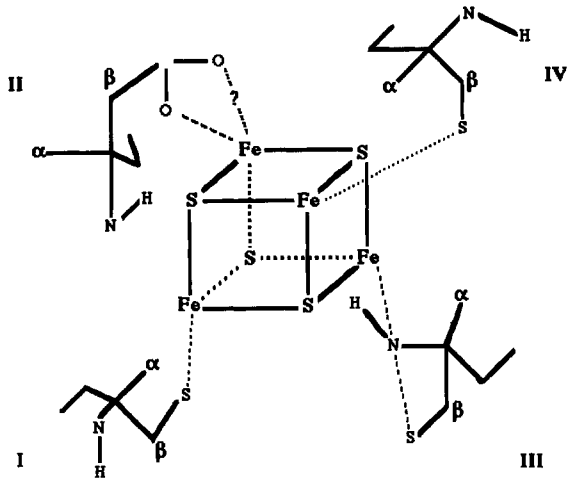

FIGURE 1: Schematic representation of the Fe_4S_4 cubane cluster with the consensus sequence ligated Cys I, III, and IV with orientation as found in crystallographically characterized bacterial type Fds. Ligand II, determined to be Asp 14 in 4Fe *Pf* Fd, is shown with the backbone as found in the Cys II ligated in common Fds. Note that Cys I and IV have C_αHs pointing toward, and NHs pointing away from, the cluster, while Cys III and Asp II have their NHs oriented toward, but the C_αH oriented away from, the cluster.

the consequences on the electronic and molecular structure, redox potential, and function for Cys substitution in natural biological cubane clusters are not understood. Similarly, ambiguous results are obtained when Cys residues are replaced using site directed mutagenesis. For example, with the 4Fe cluster (F_x) of the photosystem I reaction center, which has complete Cys ligation, replacement of one coordinating Cys by Ser gave a functional 4Fe cluster (Warren et al., 1992), but this was not the case with His or Asp substitution for the same Cys (Smart et al., 1992).

Of the 40 or so amino acid sequences known for Fds containing two cubane clusters (Matsubara & Saeki, 1992; Johnson, 1994; Moura et al., 1994), analysis of their consensus Cys sequences reveals that in several of them one of the Cys residues has been replaced, and in each case by an Asp residue (Okawara et al., 1988; Bovier-Lapierre et al., 1987; Wakabayashi et al., 1983; Minami et al., 1983; Iwasaki et al., 1994). These proteins are purified as 7Fe Fds, where the consensus sequence containing the Asp coordinates a 3Fe cluster (George et al., 1989). For single-cubane Fds, the replacement of one of the consensus Cys has been reported in proteins from only two organisms. The ferredoxins (I and II) of *Streptomyces griseolus* contain Ala at a consensus position (O'Keefe et al., 1991), and these too are purified in the 3Fe form, so their cluster status *in vivo* is not known. The other example is the 4Fe Fd from the hyperthermophile *Pyrococcus furiosus* (*Pf*), in which Asp replaces a consensus Cys (Busse et al., 1992; see Figure 2). The *Pf* protein is also unusual in that the 4Fe form is stable and does not lose Fe during purification (Aono et al., 1989; Conover et al., 1990). However, the identity of the non-Cys ligand that completes coordination to the 4Fe cluster of *Pf* Fd is unclear. Asp is just one possibility, as there is some evidence for water or hydroxide (Park et al., 1991) as found in aconitase. The 4Fe Fd from *Pf* is therefore of particular interest, as it constitutes one of the most extensively studied Fd with non-Cys ligation. It can be readily converted to the 3Fe form by ferricyanide (Conover et al., 1990a), a form which readily binds other metal ions to yield $[MFe_3S_4]$

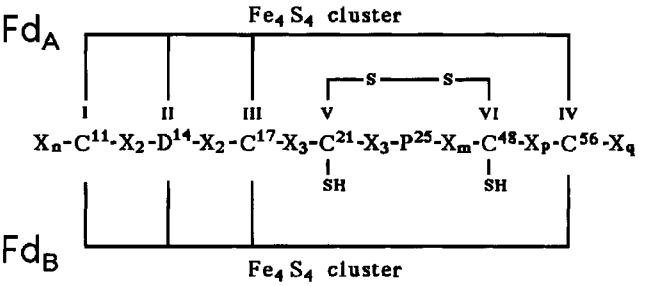

FIGURE 2: The cluster ligating consensus sequence for *Pf* Fd, with the four ligating positions I − IV occupied by Cys 11, Asp 14, Cys 17, and Cys 56, respectively. Two additional Cys, 21 and 48, are also labeled Cys V and VI. In the A form of the 4Fe *Pf* Fd (above), Cys 11(I), 14(III) 56(IV), and Asp 14(II) (as demonstrated herein) are ligated to the cluster and Cys 21(V) and Cys 48(VI) participate in a disulfide bridge. In the B form of 4Fe *Pf* Fd (below), the same four residues I−IV remain ligated to the cluster, but Cys 21(V) and 48(VI) possess free thiols (Gorst et al., 1995b).

clusters (Conover et al., 1990b; Srivastava et al., 1993; Fu et al., 1994). In addition, the 4Fe form binds ligands such as cyanide (Conover et al., 1991; Telser et al., 1995), which obviously has implications for substrate binding by complex cubane cluster containing enzymes. Moreover, reduced *Pf* 4Fe Fd exhibits a characteristic spin ground state observable by low temperature EPR that is a 9:1 mixture of $S = {}^3/_2$ and $S = {}^1/_2$, in contrast to the pure $S = {}^1/_2$ ground state for other $[Fe_4S_4]^{1+}$ clusters in most other proteins with complete Cys ligation (Conover et al., 1990a). It is not known whether this spin ground state is diagnostic for the fourth ligand, whatever that might be.

Pf 4Fe Fd possesses several other novel and unprecedented properties. The two Cys outside the cluster consensus binding sequence (Cys 21 and 48, also labeled Cys V and VI in Figure 2) form a disulfide bond which, like the Fe_4S_4 cluster, is redox active in the catalytic cycle of *Pf* Fd (Gorst et al., 1995a). A redox active disulfide has been also characterized for 3Fe Fd from *Desulfovibrio gigas* (*Dg*) (Macedo et al., 1994). However, in hyperthermophilic *Pf* 4Fe Fd, the reactivity of the disulfide bridge is so retarded at ambient temperatures that it is possible to resolve on the laboratory time scale (many hours) four redox states as shown:

$$Fd_B^{red} \xrightarrow{-e^-} Fd_B^{ox} \xrightarrow[-2H^+]{-2e^-} Fd_A^{ox} \xrightarrow{+e^-} Fd_A^{red} \xrightarrow[+2H^+]{+2e^-} Fd_B^{red} \quad (1)$$

where the superscript refers to cluster oxidation state, reduced = $[Fe_4S_4]^{+1}$, oxidized = $[Fe_4S_4]^{+2}$, and subscripts B and A refer to the established absence (*i.e.*, two Cys SH) and presence (*i.e.*, -SS-), respectively, of a disulfide bridge between Cys 21 and Cys 48.

Proton NMR has been shown to be particularly valuable in providing information not only on solution molecular structure of Fd but also on the cluster electronic/magnetic properties (Gaillard et al., 1992; Bertini et al., 1994; Teng et al., 1994; Cheng & Markley, 1995). NMR has, moreover, the potential for identifying both the type and sequence origin of the individual cluster ligands. The $[Fe_4S_4]^{+1}$ ground state is necessarily paramagnetic; that of $[Fe_4S_4]^{+2}$ is diamagnetic, but the paramagnetic $S = 1$, $S = 2$ excited states are appreciably populated at ambient temperature (Phillips & Poe, 1973; Cammack, 1992; Luchinat & Ciurli, 1993; Cheng & Markley, 1995). Hence all oxidation states of Fds exhibit

NMR spectral parameters near the cluster dominated by paramagnetic influences. The hyperfine shift,[2] δ_{hf}, can have both contact and dipolar contributions:

$$\delta_{hf} = \delta_{con} + \delta_{dip} \quad (2)$$

To date, it has generally been assumed, and on reasonable grounds, that δ_{dip} is negligible compared to δ_{con} in Fds (Phillips & Poe, 1973), which in a magnetically-coupled cluster has the following form for proton i on residue Q:

$$\delta_{con}{}^{i}(Q) = \langle S_z \rangle_Q B f(\theta_i) \quad (3)$$

where $\langle S_z \rangle_Q$ is the spin magnetization on ligand Q due to spin delocalization from iron Q, B is a constant, and $f(\theta_i)$ is an angular expression that relates to the Fe−S−C_β−H dihedral angle, θ_i, in a manner similar to the Karplus equation for three bond spin coupling in diamagnetic systems (Busse et al., 1991; Bertini et al., 1994). The nuclear relaxation rate can be qualitatively expressed:

$$T_{1i}{}^{-1} \propto (D)[S(S+1)](T_{1e}) \quad (4)$$

where D is a constant for a given state with electronic relaxation time T_{1e}. Hence, both δ_{con} and $T_{1i}{}^{-1}$ can be expected to be enhanced significantly if the $S = {}^3/_2$ ground state in $[Fe_4S_4]^{+1}$ is strongly populated when compared to the $S = {}^1/_2$ ground state.

In this report we address the ^{1}H NMR spectral properties specifically of the proton signals most strongly relaxed and hyperfine shifted by the cluster paramagnetism in the four redox states of *Pf* 4Fe Fd. Our goals are to sequence-specifically assign the signals from the three expected ligated Cys, identify the nature and sequence origin of the fourth or non-Cys ligand, analyze the magnitude of the hyperfine shifts and relaxation properties for the $[Fe_4S_4]^{+1}$ state to assess the role of an $S = {}^3/_2$ ground state, compare the electronic structure of both cluster oxidation states to those of more conventional 4Fe Fds, assess the influence of the presence or absence of the disulfide bridge on cluster electronic/molecular structure in a given cluster oxidation state, and finally, identify any properties of *Pf* Fd relevant to its electron transfer function that can be related to the nature of the non-Cys ligand.

MATERIALS AND METHODS

Pyrococcus furiosus (DSM 3638) was grown in a 600 L fermenter, and its ferredoxin (defined as *Pf* 4Fe Fd_B^{red} in the as-isolated form which contains a reduced cluster, $[Fe_4S_4]^{+1}$ and two free thiols; Gorst et al., 1995b) was purified as described previously (Aono et al., 1989). Unless noted otherwise, all procedures were carried out under strictly anaerobic conditions. The pure protein was stored frozen as pellets in liquid N_2 and was thawed when required. Where indicated, sodium dithionite was removed from samples by gel filtration (Superdex G-50) or was added to samples to reduce the protein using a Vacuum Atmosphere glovebox. Samples were reduced with excess sodium dithionite unless stated otherwise, and the pH of the samples was adjusted after addition of dithionite. pH readings were not corrected for isotope effects. Samples for NMR spectroscopy were equilibrated with 50 mM sodium phosphate buffer, pH 7.6, or with 50 mM Tris buffer, pH 8. Where indicated, samples were exchanged into 95% ^2H_2O/5% ^1H_2O in an Amicon ultrafiltration device utilizing a YM 3 membrane.

Three additional redox states of the protein were prepared as described in detail previously (Gorst et al., 1995b). 4Fe Fd_B^{ox} (oxidized cluster, $[Fe_4S_4]^{+2}$, free thiols for Cys 21, Cys 48) was prepared by treating 4Fe Fd_B^{red} with O_2 for 15 min, followed by deoxygenation and purging with Ar. 4Fe Fd_A^{ox} (oxidized cluster, $[Fe_4S_4]^{+2}$, disulfide between Cys 21, Cys 48) was prepared by treating 4Fe Fd_B^{red} with O_2 for 36 h at 30 °C followed by deoxygenation. 4Fe Fd_A^{red} (reduced cluster, $[Fe_4S_4]^{+1}$, disulfide between Cys 21, Cys 48) was prepared by treating 4Fe Fd_A^{ox} with 5-fold excess sodium dithionite for 15 min at 30 °C followed by anaerobic gel filtration.

^{1}H NMR spectra were recorded at 500 and 300 MHz on GE Omega 500 and 300 spectrometers, respectively. Chemical shift values were referenced to 2,2-dimethyl-2-silapentane-5-sulfonate (DSS) through the residual solvent signal. One-dimensional spectra were collected by the normal one-pulse with ^1H_2O presaturation or the super-WEFT (Inubishi & Becker, 1983) pulse sequence over a range of recycle times (80−500 ms). T_1 data were collected with a standard inversion−recovery pulse sequence in which recycle times were set at ~5 times the T_1 times for the peaks of interest. T_1 values were estimated from the null part in the magnetization recovery, τ_{null}, which yields $T_1 \sim \tau_{null}/\ln 2$. Steady-state NOE measurements were made using a super-WEFT pulse sequence. The selected resonance was irradiated for ~90% of the relaxation delay time. Data were acquired by interleaving a block of scans with saturation on-resonance with a block of equal scans with saturation off-resonance. The steady-state NOE (Neuhaus et al., 1989; La Mar & de Ropp, 1993), $\eta(ji)$, for a completely relaxed proton i when proton j is saturated is:

$$\eta_{j \rightarrow i} = \sigma_{ij} T_{1i} \quad (5)$$

where a strongly paramagnetically influenced T_{1i} is obtained from a nonselective inversion−recovery experiment, and σ_{ij}, the cross-relaxation rate, is given by:

$$\sigma_{ij} = (-0.1)\gamma^4 \hbar^2 r_{ij}{}^{-6} \tau_c \quad (6)$$

with r_{ij} the interproton distance. An estimated τ_c ~3 ns for the rotational correlation time of the protein yields $\sigma \sim -5$ s^{-1} for a CH_2 group (r_{ij} ~1.77 Å).

2D ^{1}H NMR experiments were performed at 500 MHz on samples which were in 50 mM phosphate, pH 7.6, in H_2O, and ranged in concentration from 5 to 8 mM. Data were collected at 30 °C over a 7017 Hz sweep width and consisted of 96 transients collected over 2048 complex points, and over 512 t_1 increments for slowly relaxing, non-hyperfine-shifted resonances. 2D TOCSY (Bax & Davis, 1985) spectra were collected at 30, 40, and 45 °C at a repetition rate of 0.5 s^{-1} and utilized an MLEV 17 spin lock applied for 60 ms. NOESY spectra were recorded with 50, 150, and 350 ms mixing times and utilized repetition rates of 0.7 s^{-1} and 0.5 s^{-1}, respectively. The water signal was suppressed with a low-power selective irradiation during the

[2] The hyperfine shift, δ_{hf}, as given by $\delta_{obs} - \delta_{dia}$, is the difference between the observed chemical shift and the expected shift in an isostructural diamagnetic complex, both referenced to DSS; δ_{dia} is 3.5 ppm for Cys, and 3.1 ppm for Asp C_βHs.

predelay period for all experiments followed by a SCUBA sequence (Brown et al., 1988) to allow for magnetization recovery of resonances close to the water frequency. For strongly relaxed and hyperfine shifted resonances, 2D NMR data were collected over a sweep width of 50.0 kHz for 4Fe Fd_B^{red} and 4Fe Fd_A^{red} and 11.0 kHz for 4Fe Fd_A^{ox} and 4Fe Fd_B^{ox}. NOESY experiments were collected using the WEFT-NOESY (Chen et al., 1994) pulse sequence with mixing times of 3 and 12 ms. The conventional n-type COSY (Bax, 1982) spectrum (MCOSY) was recorded in the magnitude mode, with 256 t_1 values of 1024 scans, each consisting of 256 t_2 points. The data were processed using a 0°-shifted sine-squared window function in both dimensions and zero-filled to 1024 × 1024 points.

NMR data were processed on either a Silicon Graphics Indigo workstation or a SUN Sparc station using the Biosym Felix 2.3 program. For data sets over 7018 Hz sweep width, 30°-shifted sine-bell-squared functions were applied in both dimensions for NOESY and TOCSY, and data sets were zero-filled to 2048 × 2048 real data points prior to Fourier transformation.

RESULTS

Temperature, Solvent, and pH Influences on Spectral Parameters. The normal 30 °C ^{1}H NMR spectra of the four 4Fe Fd complexes of interest, with reduced, $[Fe_4S_4]^{+1}$, cluster, Fd_B^{red}, and Fd_A^{red}, and with oxidized, $[Fe_4S_4]^{+2}$, cluster, Fd_A^{ox} and Fd_B^{ox}, are illustrated in Figures 3B, 4A, 5A (with expansion of the 4.6−5.8 ppm region in Figure 6A) and Figure 5F, respectively. Comparison of spectra in ^1H_2O and ^2H_2O (after prolonged incubation) leads to identification of all resolved nonexchangeable *vs* exchangeable resonances (see Figure 5A,B′ and supporting information). The labeling of resonances is defined for the spectrum with the most resolved resonances, that of the reduced B form or Fd_B^{red}, and uses the convention B_i^r, b_i^r, where upper and lower case letters designate nonlabile and labile protons, respectively, the superscript r designates the reduced cluster, $[Fe_4S_4]^{+1}$, and the subscript i is indexed at $(1 - n)$ for all resonances experimentally adddressed in this report, with i increasing with the upfield direction of the chemical shift (see Figure 3A,B). The same convention is used to label the peaks for Fd_A^{red} (A_i^r, a_i^r; Figure 4A), Fd_A^{ox} (A_i^o, a_i^o; see Figure 5A), and Fd_B^{ox} (B_i^o, b_i^o; see Figure 5F), where the index i for a signal is the same as that for $4Fe_B^{red}$ only when the signal can be assigned to the same proton. The chemical shifts for all resolved protons which exhibit significant paramagnetic relaxation and/or hyperfine shifted influences are listed in Table 1 for the reduced cluster, $[Fe_4S_4]^{+1}$, in proteins Fd_B^{red} and Fd_A^{red}, and in Table 2 for the oxidized cluster, $[Fe_4S_4]^{+2}$, in proteins Fd_A^{ox} and Fd_B^{ox}. The nonselective T_1 values for resolved and partially resolved signals for the four species are included in Tables 1 and 2.

The chemical shifts for the two extreme redox forms, Fd_A^{ox} and Fd_B^{red}, are found essentially independent[3] of pH over the region 5.0−8.5 (data not shown) and indicate that the pK previously observed in 3Fe Fd_A^{ox}, and attributed to the

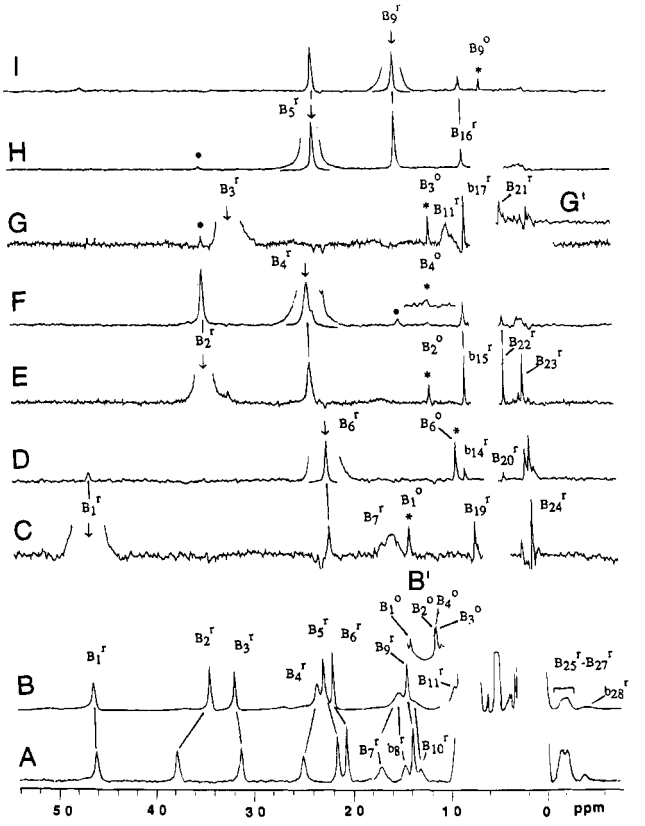

FIGURE 3: Resolved portions of the 500 MHz ^{1}H NMR reference spectra (repetition rate 0.33 s^{-1}) of ~8 mM 4Fe *Pf* Fd_B^{red} (as isolated with reduced cluster $[Fe_4S_4]^{+1}$ and free thiols for Cys 21, 48) in 90% ^1H_2O/10% ^2H_2O, 50 mM phosphate, pH 8.0, at (A) 50 °C and (B) 30 °C. The resonances are labeled by subscript i starting at low field, for nonlabile (B_i^r) and labile (b_i^r) proton signals for the B form, with superscript r to denote the reduced cluster. (B′) exhibits the new peaks due to 4Fe *Pf* Fd_B^{ox} with peak B_i^o (oxidized cluster, $[Fe_4S_4]^{+2}$, with free thiols for Cys 21, 48) upon rapid but only partial oxidation by O_2. (C)−(I) are difference traces at 30 °C by saturation of the B_i^r resonance in *Pf* Fd_B^{red} (with vertical arrow) in the sample with ~25% 4Fe *Pf* Fd_B^{ox} present. The peaks in the difference traces marked by asterisks (and B_i^o label) are observed only when *Pf* Fd_B^{ox} is present and reflect saturation transfer via intermolecular electron transfer; all other peaks arise from NOEs with 4Fe Fd_B^{red} and are similarly labeled B_i^r, b_i^r. The upfield portion of difference trace G in ^2H_2O is shown in inset G′; off-resonance effects are identified by the symbol •.

Asp 14 form (Gorst et al., 1995a), is not present in 4Fe Fd_A^{ox}. The temperature dependence of the chemical shifts for Fd_A^{red} and Fd_B^{red} are illustrated in panels A and B, respectively, of Figure 7, in the form of Curie plots; the sign of the slope and sign of the hyperfine shift lead to the designations Curie and anti-Curie for hyperfine shift which decrease and increase, respectively, with increasing temperature. The chemical shifts for all hyperfine shifted resonances in 4Fe Fd_A^{ox} and Fd_B^{ox} exhibit anti-Curie behavior (not shown, see supporting information).

Location of Signals for Ligated Residues. Initially, we focused on locating hyperfine shifted signals which can be established to arise from different ligands, in that the location of four such sets of signals clearly dictates that we have detected the fourth or non-Cys ligand. It is also necessary to demonstrate that the signals for four such residues are detectable in all four species. The criteria for locating the signals for cluster ligands (initially labeled ligands **I**−**IV**) are that the signals exhibit significant temperature-dependent hyperfine shifts and strong paramagnetic relaxation (short

[3] While the hyperfine shifts exhibited no pronounced pH effects indicative of a titrating group, small shift changes were observed that could be attributed to buffer and/or ionic strength effects and solvent isotope. These effects, however, are relatively small, and their origin was not investigated in detail.

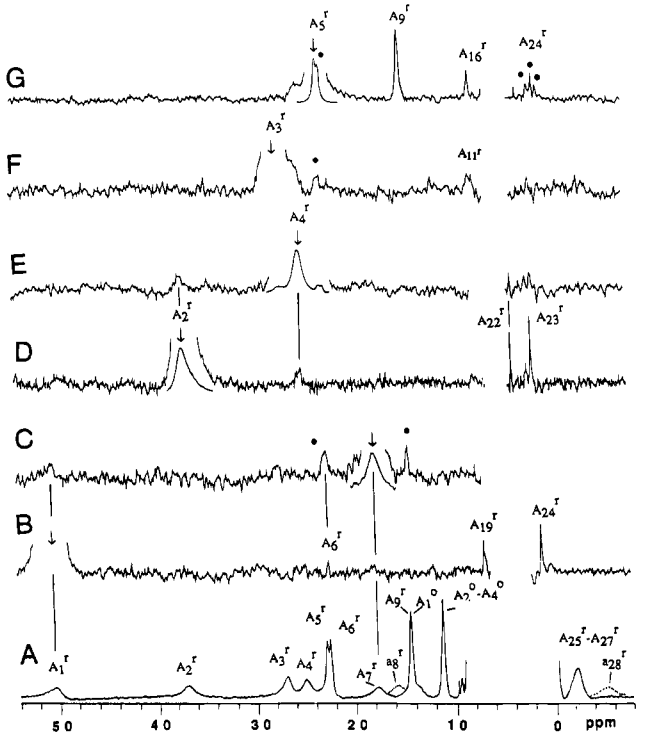

FIGURE 4: (A) Resolved portions of the 500 MHz ^{1}H NMR reference spectrum (repetition rate 0.33 s^{-1}) of ~4 mM 60% Fd_A^{red} with peak A_i^r ($[Fe_4S_4]^{+1}$ and disulfide between Cys 21, 48) and 40% Fd_A^{ox} with peaks A_i^o ($[Fe_4S_4]^{+2}$ and free thiols for Cys 21, 48) in ^2H_2O at 30 °C, 50 mM phosphate, pH 8.0; the positions of hyperfine shifted labile proton peaks a_8^r, a_{28}^r for Fd_A^{red} (observed in ^1H_2O) are shown by dotted lines. (B)−(G) are NOE difference traces obtained by saturating the A_i^r peak of Fd_A^{red} as indicated by vertical arrow. Resonances observed in the difference traces arise solely from intramolecular NOEs, and the resonances are labeled A_i^r; no saturation transfer from Fd_A^{red} to Fd_A^{ox} is observed at 30 °C. Off-resonance effects are identified by the symbol •.

T_1s). Extensive assignments necessary to locate the four residues have been carried out on Fd_B^{red} and Fd_A^{ox}; sufficient assignments are extended to Fd_A^{red} and Fd_B^{ox} to show the four residues remain coordinated and to cross-correlate the assignments among all four species. The ligated Cys would be expected to exhibit three hyperfine shifted $C_\beta H_2-C_\alpha H$ fragments whose diagnostic feature is expected to be a strongly shifted and relaxed geminal proton pair (*i.e.*, $C_\beta H_2$) that is readily and uniquely detected by a steady-state NOE.

The optimally resolved 500 MHz spectrum at 30 °C for the as-isolated Fd_B^{red} (reduced cluster $[Fe_4S_4]^{+1}$ with free thiols for Cys 21, 48) in ^1H_2O is shown in Figure 3B, with nonlabile and labile proton signals labeled B_i^r and b_i^r, respectively; the trace at 50 °C allows resolution of B_7^r (nonlabile) and b_8^r (labile), as shown in Figure 3A. 2D correlation (MCOSY) experiments establish scalar connectivities for $B_1^r-B_6^r$, $B_1^r-B_7^r$, $B_2^r-B_4^r$, $B_2^r-B_{25}^r$, $B_3^r-B_{11}^r$, $B_5^r-B_9^r$, $B_5^r-B_{16}^r$, and $B_9^r-B_{16}^r$, while 2D dipolar (NOESY) correlation yields the connectivities $B_1^r-B_7^r$, $B_2^r-B_4^r$, $B_3^r-B_{11}^r$, $B_5^r-B_9^r$, and $B_5^r-B_{16}^r$ (data not shown; see supporting information). Hence 2D NMR locates three three-spin and one two-spin systems with significant hyperfine shifts and paramagnetic relaxation (Table 1). The cross peak intensities, however, do not clearly distinguish between geminal and vicinal coupling between proton pairs because of different relaxation properties. The steady-state NOEs resulting from saturation of peak $B_1^r-B_9^r$ for Fd_B^{red}, which allows these assignments, are illustrated in Figure 3C−I. The

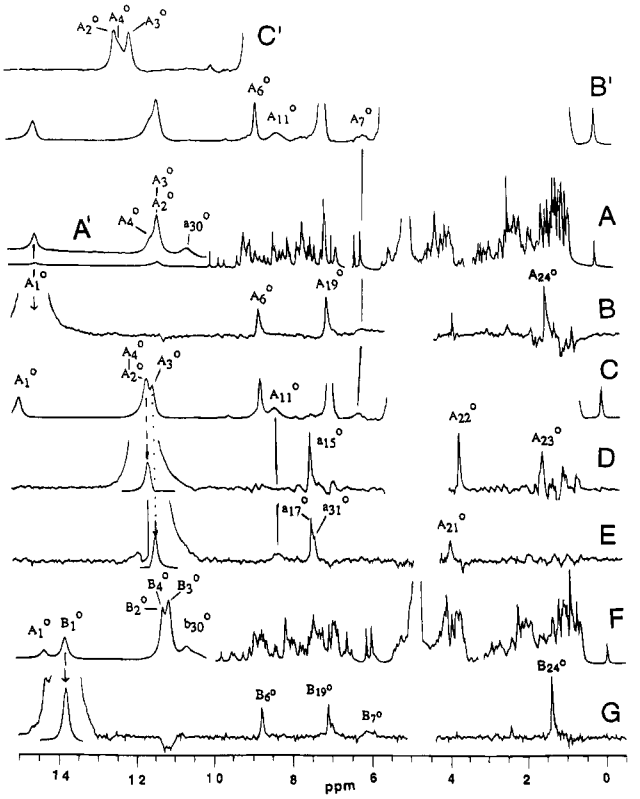

FIGURE 5: (A) Reference 500 MHz ^{1}H NMR spectrum of ~8 mM *Pf* Fd_A^{ox} ($[Fe_4S_4]^{+2}$, disulfide between Cys 21, 48) in 90% ^1H_2O/10% ^2H_2O, 50 mM phosphate, pH 7.3 at 30 °C, with proton peaks labeled A_i^o (nonlabile), a_i^o (labile); the vertical scaling of 0−3.5 ppm is 1/4 times that of 3.5−15 ppm. (A′) The section 9−15 ppm with 5 times vertical expansion. (B′) Super-WEFT spectrum (4 s^{-1}, 100 ms relaxation delay) in ^2H_2O at 30 °C in a well exchanged sample that identifies an additional three strongly relaxed and hyperfine shifted nonlabile protons A_6^o, A_7^o, A_{11}^o. (C′) Super-WEFT spectrum in ^2H_2O at 80 °C which shows the three proton composite at 30 °C can be partially resolved at three signals A_2^o, A_3^o, A_4^o with differential relaxation times. (B) NOE difference trace resulting from saturation of peak A_1^o (vertical arrow) of Fd_A^{ox} at 30 °C, with resulting NOEs to peaks labeled A_i^o. (C) 500 MHz super-WEFT trace from Fd_A^{ox} in 90% ^1H_2O/10% ^2H_2O at 50 °C which partially resolves peak A_3^o from a composite of A_2^o, A_4^o. (D, E) NOE difference traces at 50 °C upon saturation of the composite A_2^o, A_4^o (D) and A_3^o (E); resulting NOEs are labeled A_i^o (nonlabile) and a_i^o (labile) protons. Note off-resonance saturation of the adjacent resonances has been computer corrected in each case. (F) 500 MHz reference trace (0.33 s^{-1}) of 5 mM 75% Fd_B^{ox} (peak B_i and b_i), 25% Fd_A^{ox} (peak A_i^o, a_i^o) in 90% ^1H_2O/10% ^2H_2O, 50 mM phosphate, pH 7.3 at 30 °C. (G) NOE difference trace upon saturating B_i^o of Fd_B^{ox}; NOEs are labeled B_i^o. Off-resonance effects are identified by the symbol •.

magnitudes of the NOEs, together with the T_1s in Table 1, reveal four sets of geminal protons[4] (r_{ij} = 1.77 Å → $\sigma \sim -5$ s^{-1} via eq 5): partners $B_1^r-B_7^r$ (Figure 3C), $B_2^r-B_4^r$ (Figure 3E,F), $B_3^r-B_{11}^r$ (Figure 3G), and $B_5^r-B_9^r$ (Figure 3H,I), and confirm vicinal (r_{ij} ~2.5 Å via eqs 5 and 6) partners $B_1^r-B_6^r$ (Figure 3C,D) and $B_9^r-B_{16}^r$ (Figure 3I). Hence the four ligands are labeled ligand I (B_2^r, B_4^r, B_{25}^r), ligand II (B_5^r, B_9^r, B_{16}^r), ligand III (B_1^r, B_7^r, B_6^r), and ligand IV (B_3^r, B_{11}^r), with the three resonances reflecting $C_\beta H_2-C_\alpha H$ fragments for ligands I, III, and IV; for ligand IV the $C_\alpha H$ is undetected.

[4] The most "unusual" geminal proton pair is that for the narrow and only moderately relaxed proton pair B_5^r, B_9^r, where the $T_1(B_9^r)$ of ~22 ms and the −16% steady-state NOE yield σ = 4.9 s^{-1}. These data demand that they arise from a CH_2 group.

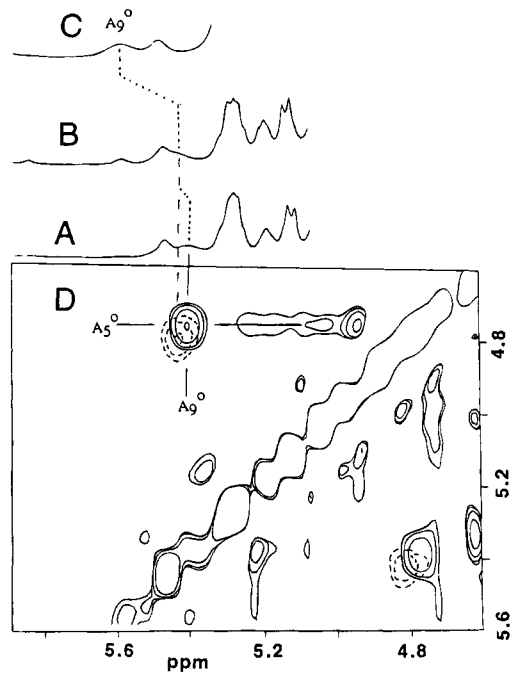

FIGURE 6: Portions of the 500 MHz ^{1}H NMR spectrum of 8 mM *Pf* Fd_A^{ox} at (A) 39, (B) 45, and (C) 80 °C, respectively, in ^2H_2O, 50 mM phosphate, pH 7.5, which identify a strongly relaxed (T_1 ~15 ms) hyperfine shifted nonlabile proton peak $A_9°$ which displays strong anti-Curie behavior. (D) TOCSY (τ_m = 15 ms) cross peak at 39 °C which aligns with peak $A_9°$ (and tracks peak $A_9°$ at 45 °C as shown by the position of this cross peak at 45 °C in dashed lines).

Table 1: Spectral Properties of Protons for Hyperfine Shifted and/or Strongly Relaxed Protons in *Pyrococcus furiosus* 4Fe Fd^{red} with Reduced Cluster

		Fd_A^{red} (disulfide for Cys 21, 48)			Fd_B^{red} (free SH for Cys 21, 48)		
	proton	label[a]	shift[b]	T_1[c]	label[d]	shift[b]	T_1[c]
ligand I (Cys 11)	$C_\beta H$	A_2^r	37.4	14	B_2^r	34.7	19
	$C_{\beta'}H$	A_4^r	25.3	6	B_4^r	23.8	9
	$C_\alpha H$	A_{25}^r	*e*		B_{25}^r	−2.0	~3
	NH	a_{15}^r	*e*		b_{15}^r	7.61	~60
ligand III (Cys 17)	$C_\beta H$	A_1^r	50.2	10	B_1^r	45.8	13
	$C_{\beta'}H$	A_7^r	17.5	3	B_7^r	15.2	3
	$C_\alpha H$	A_6^r	22.4	21	B_6^r	21.8	29
ligand IV (Cys 56)	$C_\beta H$	A_3^r	27.0	14	B_3^r	31.6	17
	$C_{\beta'}H$	A_{11}^r	7.5	*f*	B_{11}^r	9.35	<5
	NH	a_{17}^r	*e*		b_{17}^r	7.35	60
ligand II (Asp 14)	$C_\beta H$	A_5^r	22.8	14	B_5^r	22.7	21
	$C_{\beta'}H$	A_9^r	14.4	17	B_9^r	14.3	15
	$C_\alpha H$	A_{16}^r	7.38	*f*	B_{16}^r	7.46	*f*
others		a_8^r	14.2	~7	b_8^r	15.2	6
		A_{10}^r	12.8	~5	B_{10}^r	13.7	~3
		A_{26}^r	−2.1[g]		B_{26}^r	−2.2[g]	~3
		A_{27}^r	−2.1[g]	B_{27}^r	−2.2[g]	~3	
		a_{28}^r	−4.2	~3	b_{28}^r	−4.3	~3

[a] Peak labels as in Figure 4A. [b] Chemical shifts in ppm at 30 °C in ^1H_2O, referenced to DSS. [c] T_1 values in ms; uncertainty ~±15%. [d] Peak labels as in Figure 3B. [e] Not assigned. [f] Not determined. [g] Unresolved composite.

The 30 °C ^{1}H NMR spectrum of *Pf* Fd_A^{red} in ^2H_2O $([Fe_4S_4]^{+1}$ with a disulfide bond between Cys 21, 48), with peaks A_i^r, exhibits much broader lines than Fd_B^{red} (compare Figure 4A to Figure 3B), but a very similar shift pattern and T_1 values (see Table 1). The larger linewidths of Fd_A^{red} at 30 °C reflect an exchange contribution[5] which is suppressed at higher temperature, where the linewidth of Fd_B^{red} and

Table 2: Spectral Properties of Protons for Hyperfine Shifted and/or Strongly Relaxed Protons in *Pyrococcus furiosus* 4Fe Fd with Oxidized Cluster

		Fd_A^{ox} (disulfide for Cys 21, 48)			Fd_B^{ox} (free Cys 21, 48)		
	proton	label[a]	shift[b]	T_1[c]	label[d]	shift[b]	T_1[c]
ligand I (Cys 11)	$C_\beta H$	$A_2°$	11.3	~9[e]	$B_2°$	11.3	10
	$C_{\beta'}H$	$A_4°$	11.1	~3[e]	$B_4°$	11.1	*f*
	NH	$a_{15}°$	7.49	*f*	$b_{15}°$	7.35 or 7.42	*f*
ligand III (Cys 17)	$C_\beta H$	$A_1°$	14.3	6	$B_1°$	13.8	*f*
	$C_{\beta'}H$	$A_7°$	5.9	2	$B_7°$	6.0	*f*
	$C_\alpha H$	$A_6°$	8.6	33	$B_6°$	8.75	*f*
ligand IV (Cys 56)	$C_\beta H$	$A_3°$	11.1	9[e]	$B_3°$	11.1	*f*
	$C_{\beta'}H$	$A_{11}°$	8.1	4	$B_{11}°$	8.2	*f*
	NH	$a_{17}°$	7.49	*f*	$b_{17}°$	7.42 or 7.35	*f*
ligand II (Asp 14)	$C_\beta H$	$A_5°$	4.9	*f*	$B_5°$	4.9	*f*
	$C_{\beta'}H$	$A_9°$	5.37	15	$B_9°$	5.37[g]	*f*
others		$a_{30}°$	9.0	3	$b_{30}°$	9.2	3

[a] Peak labels as in Figures 5A and 8A. [b] Chemical shifts in ppm at 30 °C in ^1H_2O, referenced to DSS. [c] T_1 values in ms. [d] Peak labels as in Figure 5F. [e] Determined at 70 °C, where $A_2°$, $A_3°$, $A_4°$ are sufficiently resolved. [f] Not sufficiently resolved to allow estimates. [g] Chemical shift at 40 °C in ^1H_2O, referenced to DSS.

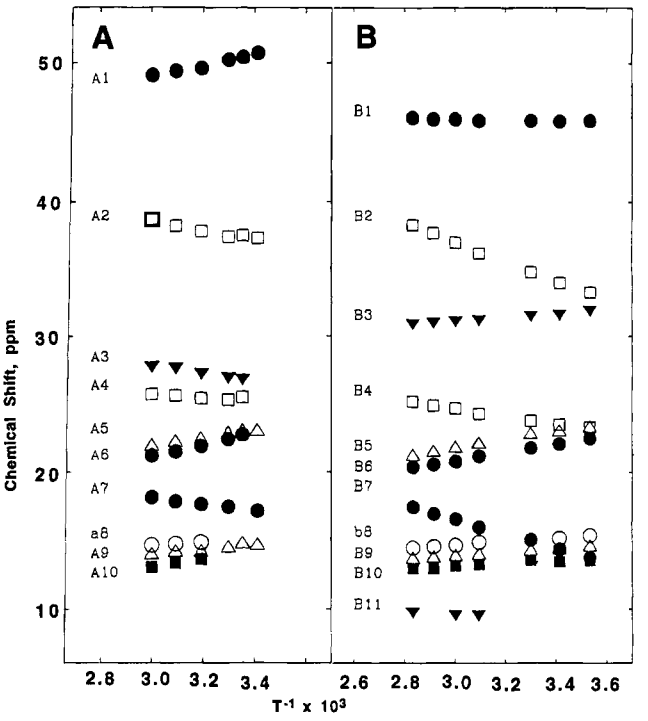

FIGURE 7: Curie plots (chemical shift, referenced to DSS, *vs* reciprocal absolute temperature) for low-field hyperfine shifted and relaxed resonances for the following: (A) *Pf* Fd_A^{red} $([Fe_4S_4]^{+1}$ with free thiols for Cys 21, 48) with proton peaks A_i^r (nonlabile), a_i^r (labile), as labeled in Figure 4; and (B) *Pf* Fd_B^{red} $([Fe_4S_4]^{+1}$ with disulfide bridge between Cys 21, 48), with B_i^r (nonlabile), b_i^r (labile) proton peaks. The resonances belonging to the four ligands are given by the same symbols (□ for Cys 11, △ for Asp 14, ● for Cys 17, and ▼ for Cys 56) in both panels. Positive and negative slopes are designated Curie and anti-Curie, respectively.

Fd_A^{red} are essentially the same (not shown; see supporting information). Since Fd_A^{red} converts to Fd_B^{red} at elevated temperatures (likely by disproportionation to Fd_B^{red} and Fd_A^{ox}; Gorst et al., 1995b), steady-state NOEs on *Pf* Fd_A^{red} are carried out at 30 °C and in ^2H_2O solution. Saturation of peak A_1^r (Figure 4B) and A_7^r (Figure 4C) locate one $C_\beta H_2$-

$C_\alpha H$ fragment (A_1^r, A_7^r, A_6^r), while irradiating A_2^r, A_4^r (Figure 4D,E), A_3^r (Figure 4F; to geminal partner A_{11}^r), and A_5^r (Figure 4G; geminal partner A_9^r and vicinal partner to A_{16}^r) locates geminal proton pairs of three other hyperfine shifted residues; hence four residues are ligated. The chemical shifts and T_1 values for Fd_A^{red} are included in Table 1. We note a very close similarity in hyperfine shift and relaxation pattern for the signals of the *four* ligated residues observed for Fd_B^{red} (Figure 3) and Fd_A^{red} (Figure 4) and hence assign similarly labeled peaks to the same residues (*i.e.*, ligand III = A_1^r, A_6^r, A_7^r in Fd_A^{red} and B_1^r, B_6^r, B_7^r in Fd_B^{red}, etc., as shown in Table 1). These correlations will be confirmed via sequence-specific assignments below.

The ^1H NMR spectra for the proteins with an oxidized cluster, Fd_A^{ox} or Fd_B^{ox}, are not as well resolved as for the reduced cluster Fds, as shown in panels A and F, respectively, of Figure 5. Both exhibit a single proton peak near 14 ppm (A_1, B_1) and a composite of three peaks (one broad A_4 (or B_4) and two narrow A_2, A_3 (or B_2, B_3)), as shown resolved at 80 °C for Fd_A^{ox} (Figure 5C′). The resonances of Fd_B^{ox} (oxidized cluster, $[Fe_4S_4]^{+2}$, free SHs for Cys 21, 48), however, could be definitively assigned on the basis of saturation transfer from the assigned B_i^{red} peaks of Fd_B^{red} to the B_i^{ox} peaks of Fd_B^{ox}, also as shown in Figure 3. The effect on the ^1H NMR spectra of generating ~20% Fd_B^{ox} upon admitting limited O_2 to Fd_B^{red} is shown in the inset Figure 3B′; the peaks for Fd_B^{ox} are labeled B_i^o. Saturation of peaks for Fd_B^{red} in the presence of Fd_B^{ox} yields peaks indicated with a star (* in Figure 3C−I); they are absent for pure Fd_B^{red} and/or vary in intensity with the amount of Fd_B^{ox} present (data not shown). Saturation of peaks B_1^r−B_4^r, B_6^r, and B_9^r in Fd_B^{red} leads to the location of peaks B_1^o−B_4^o, B_6^o, and B_9^o in Fd_B^{ox} (Figure 3C−G,I); saturation of B_5^r leads to cross saturation of B_5^o near the solvent resonance (4.9 ppm) detected only in ^2H_2O (not shown). Direct saturation of B_1^o in pure Fd_B^{ox} in Figure 5G provides the confirming NOE to vicinal partner B_6^o and locates the geminal partner B_7^o. Note that the saturation transfer for Fd_B^{red} to Fd_B^{ox} provides the signals correlated with ligands I−IV defined for Fd_B^{red}. The chemical shifts and T_1s are listed in Table 2, and variable temperature properties (all anti-Curie) are found in the supporting information.

The 500 MHz ^1H NMR spectrum of Fd_A^{ox} (oxidized cluster, $[Fe_4S_4]^{+2}$, with disulfide bridge between Cys 21, 48) exhibits only one resolved peak, A_1^o, and a composite for three protons, A_2^o−A_4^o, outside the diamagnetic envelope in ^1H_2O (Figure 5A; vertical expansion in Figure 5A′). However, a WEFT spectrum designed to detect rapidly relaxed protons on a ^2H_2O exchanged sample reveals three more strongly relaxed resonances A_6^o, A_7^o, and A_{11}^o (Figure 5B′), and variable temperature shows that the set A_2^o−A_4^o can be at least partially resolved (Figure 5C′). 2D NOESY spectra exhibit weak cross peaks A_1^o−A_6^o, A_1^o−A_7^o, and A_3^o−A_{11}^o for resolved peaks but fail to identify CH_2 groups (not shown; see supporting information). Attempts to cross correlate the assignments for Fd_A^{red} in Figure 4 to Fd_A^{ox} (each with disulfide bridge between Cys 21, 48) via saturation transfer under conditions comparable to those for the pair Fd_B^{ox}, Fd_B^{red} (each with free SHs for Cys 21, 48) failed at 30 °C. Detectable saturation transfer is observed only at much higher temperatures (*i.e.*, 70 °C), but under these conditions, chemical conversion of Fd_B^{ox} to Fd_A^{ox} is also strongly accelerated (Gorst et al., 1995b). At 70 °C, it was possible to detect direct saturation transfer only from peak A_9^r of Fd_A^{red} to the above assigned A_9^o of Fd_A^{ox} (not shown). The remaining assignments, however, can be pursued directly on Fd_A^{ox}.

Saturation of A_1^o at 30 °C yields NOEs to A_6^o and A_7^o that the T_1 estimates dictate (via eqs 5 and 6) are vicinal and geminal partners, respectively, to A_1^o. The reference spectrum of Fd_A^{ox} in ^1H_2O at 50 °C shows that peak A_3^o is partially resolved from the composite of A_2^o, A_4^o (Figure 5C). Saturation of the composite A_2^o, A_4^o fails to result in an NOE to other relaxed nonlabile proton resonances (Figure 5D), but saturation of A_3^o results in an NOE to nonlabile and relaxed proton A_{11}^o indicative of geminal protons (Figure 5E). A reasonable hypothesis at this point is that we have identified the geminal protons for one ligand A_3^o, A_{11}^o (later shown to be ligand IV) and both the geminal and vicinal protons of one ligand A_1^o, A_7^o, A_6^o (later shown to ligand III) and that the failure to observe NOEs from either A_2^o, A_4^o to other relaxed nonlabile proton resonances dictates that they arise from the geminal protons of the third ligand (later shown to be ligand I). Careful inspection of the poorly resolved 5.0−5.5 ppm ^1H NMR spectra of Fd_A^{ox} as a function of temperature reveals one other peak, A_9^o, with strong anti-Curie behavior (Figure 6A−C), whose T_1 ~15 ms (Table 1) also indicates a ligand origin. Portions of a 15 ms TOCSY map at two temperatures (Figure 6D) exhibit a strong cross peak between A_9^o and A_5^o, indicative of a hyperfine shifted CH_2 fragment of the fourth ligand (later shown to be ligand II). The geminal nature of peaks A_9^o−A_5^o is confirmed by the strong NOESY peak observed for τ_m = 15 ms (see supporting information). The four located CH_2 fragments must arise from the four ligands; the correlations to ligands I−IV of Fd_B^{red} remain to be established.

Sequence-Specific Ligand Assignments. The unambiguous assignment of ligated residues, particularly in view of an incompletely defined tertiary structure of *Pf* Fd (Gorst et al., 1995b), demands the detection of dipolar connectivities between the backbone protons ($C_\alpha H$, N_pH) of cluster ligands and nearby noncoordinated residues and, hence, requires NOE data in ^1H_2O solution (Wüthrich, 1986). Standard 2D TOCSY (τ_m 60 ms) and NOESY (τ_m 150, 250 ms) experiments suited for "diamagnetic" protons carried out on both Fd_B^{red} and Fd_A^{ox} lead to spin system identification and sequence-specific assignment of several residues relatively unaffected by the cluster paramagnetism. The assignment strategy and resulting chemical shifts are very similar to those presented in detail for *Pf* 3Fe Fd^{ox} (Teng et al., 1994). The critical residues are Gln 8, Asp 9, and Thr 10 near Cys 11 (see Figures 2 and 8), the segment AMX-Leu-AMX which identifies Leu 20 near Cys 17, and Ser 59 which exhibits the characteristic spin system and no cross peaks in the NOESY map (Teng et al., 1994); the backbone proton chemical shifts for these "diamagnetic" residues are listed in Table 3. In considering the assignments of ligated residues, we take advantage of the earlier observation (Gorst et al., 1995a) that cubane clusters in structurally characterized

[5] The strong temperature dependent linewidths have been observed in the A form (disulfide between Cys 21, Cys 48), but not the B form (free thiols for Cys 21, Cys 48), of the *Pf* 3Fe Fd^{ox}; in the A form it was possible to "freeze" out two sets of hyperfine shifted signals at very low temperatures (5 °C) (Busse et al., 1992). For *Pf* 4Fe Fd_A^{red}, the lowest temperature used (5 °C) failed to resolve the contributing resonances.

Table 3: Chemical Shifts of Nonligated Residues in *Pyrococcus furiosus* 4Fe Ferredoxins

		4Fe Fd_B^{red}		4Fe Fd_A^{ox}		3Fe Fd^{ox}
residue	proton	label[a]	shift[b]	label[c]	shift[b]	shift[d]
Gln 8	NH	b_{12}^r	8.65		8.78	8.99
	$C_\alpha H$		3.56		*e*	3.80
Asp 9	NH	b_{13}^r	8.03		8.33	8.18
	$C_\alpha H$		4.45		4.44	4.54
Thr 10	NH	b_{18}^r	7.06		7.25	7.37
	$C_\alpha H$		4.05		4.09	4.13
Leu 20	NH	b_{14}^r	7.81		*e*	8.34
	$C_\alpha H$		4.16		*e*	4.19
Ser 59	NH	b_{31}^r	*e*	a_{31}^o	7.33[f]	7.06
	$C_\alpha H$		*e*		4.57[f]	4.72
Phe 25	ring	B_{19}^r	7.00	A_{19}^o	6.98	6.91
others		B_{20}^r	3.76	A_{20}^o	3.82	3.78
		B_{21}^r	3.56	A_{21}^o	3.93	3.80
		B_{22}^r	3.55	A_{22}^o	3.60	3.80
		B_{23}^r	1.60	A_{23}^o	1.60	1.10
		B_{24}^r	1.07	A_{24}^o	1.05	1.13

[a] Peak labels as defined in Figures 3A, 3B, and 8B. [b] Shift at 30 °C in ^1H_2O in ppm from DSS. [c] Peak labels as defined in Figure 5A–F. [d] Shifts at 30 °C in ^1H_2O, in ppm from DSS (taken from Teng et al., 1994). [e] Not assigned. [f] Shift at 50 °C in ^1H_2O in ppm from DSS.

Fds (Adman et al., 1976; Fukayama et al., 1988; Stout, 1989; Backes et al., 1991; Kissinger et al., 1991) exhibit largely conserved, and pseudo-twofold ligation geometry (Figure 1) about the cluster where Cys I and Cys IV have the $C_\alpha H$ very close (≤4 Å) to the cluster, and the NH remote from the cluster (≥5 Å) but close (~2.5 Å) to the Cys C_βHs; hence the NHs are readily detectable by NMR. In contrast, Cys II and Cys III are oriented to exhibit severely broadened NHs close to Fe, but relatively narrow C_αHs distant (~5 Å) from the iron, and hence readily detectable by ^1H NMR (Gorst et al., 1995a).

We initiate these sequence-specific assignments in Fd_B^{red} (Figure 3). The NOE from ligand III $C_\alpha H$ to labile proton peak b_{14}^r (Figure 3D), assigned by standard 2D NMR as the Leu 20 NH, identifies ligand III as Cys 17; this is confirmed by the NOE from B_1^r (Cys 17 $C_\beta H$) to B_{19}^r (Phe 25 ring H; Figure 3C). The NH of Cys 17 could not be located, which is consistent with its expected severe relaxation. Saturation of signals B_2^r, B_4^r (Figure 3E,F) of ligand I and B_3^r of ligand IV (Figure 3G) results in ~−3 ± 1% NOEs to labile protons b_{15}^r and b_{17}^r, respectively, identifying the peptide NHs (T_1 ~60 ms yields r_{ij} ~2.5 Å via eqs 5 and 6) for these two residues and collectively identifying ligands I and IV as arising from Cys 11 and Cys 56. The NOE from B_2^r to b_{15}^r (ligand I) is expanded in Figure 8A, where it is aligned with a NOESY cross peak (Figure 8B) observed at 50 but not 200 ms mixing times that is due to peak b_{18}^r (assigned as Thr 10 NH) as found in the 3Fe form (Teng et al., 1994). Thr 10, in turn, is readily identified by its characteristic backbone NH connectivity to Asp 9 (b_{13}^r), which in turn is connected to Gln 8 (b_{12}^r), as shown in Figure 8B. Hence ligand I is clearly Cys 11, and therefore ligand IV must be Cys 56 (confirmed below). Saturation of peaks B_5^r and B_9^r failed to yield NOEs to any assigned resonance and, hence, leaves the scalar connected three-spin system of ligand II as unassigned at this time.

These same sequence-specific assignments of ligands I, III, and IV are trivially obtained for Fd_B^{ox} by observing saturation transfer from the Fd_B^{red} peaks to Fd_B^{ox} peaks (peaks with asterisks in Figure 3C–I) and lead to the chemical shifts

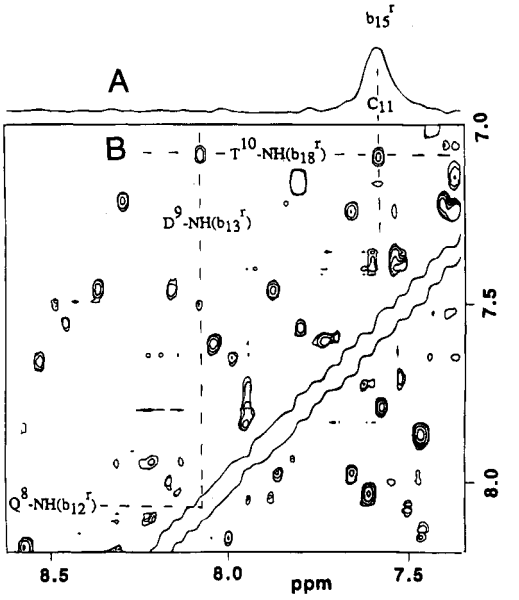

FIGURE 8: (A) Portion of the 500 MHz NOE difference trace for 8 mM *Pf* Fd_B^{red} in 90% ^1H_2O/10% ^2H_2O, 150 mM phosphate, at 30 °C, upon saturating peak B_2^r, which locates the peptide NH (peak b_{15}^r) for the ligand. (B) Portion of the τ_m = 50 ms NOESY spectrum of the sample which illustrates NH–NH connectivities for adjacent residues. The cross peak between b_{15}^r and b_{18}^r (Thr 10 NH), observed at τ_m 50 but not 250 ms, identifies B_2^r and b_{15}^r as arising from Cys 11. The NH connectivities Thr 10 (b_{18}^r)–Asp 9 (b_{13}^r)–Gln 8 (b_{12}^r) are also shown.

(and, when resolved, T_1s) for the latter complex of at least the C_βHs for the three Cys as well as the unassigned ligand II.

In the case of Fd_A^{ox} in ^1H_2O at 50 °C, saturation of resonances for both ligand I (peak A_2^o, A_4^o; Figure 5D) and ligand IV (peak A_3^o; Figure 5E) yields moderate intensity NOEs to two peptide NHs (*i.e.*, labile proton peaks a_{15}^o and a_{17}^o in panels D and E, respectively, of Figure 5), locating collectively the Cys 11 and Cys 56 peptide NHs. However, saturation of A_3^{ox} also yields a weaker NOE to another labile proton peak labeled a_{31}^o in Figure 5E, which TOCSY identifies uniquely as the NH of Ser 59. This leads directly to the assignment of ligand IV to Cys 56, and therefore ligand I to Cys 11 for Fd_A^{ox}. The NOE for ligand III peak A_1^o to A_{19}^o, the Phe 25 ring H, confirms ligand III as Cys 17, and leaves ligand II as the non-Cys ligand (Teng et al., 1994). The chemical shifts, their variable temperature slopes, and T_1 values for Fd_A^{ox} and Fd_B^{ox} are listed in Table 2.

Cluster Tertiary Contacts. Saturation of the hyperfine shifted peaks for each complex yields, in addition to the data used above to locate the various protons on a given ligand and the sequence-specific assignment of the three Cys, NOEs to several weakly relaxed protons in the aliphatic spectral window (4.5 to 0 ppm) that reflect the contacts between the cluster ligands and the protein matrix. The origins of these residues are unknown at this time and require much more extensive data and analysis. However, it is noted that the same assigned Cys C_βHs exhibit very similar patterns[6] of such "tertiary" NOEs in the various redox states. The

[6] Note that similar peaks are also observed in the 0–4.5 ppm window in the two "intermediate" species 4Fe Fd_A^{red} (peaks A_{19}^r–A_{24}^r in Figures 4B, 4D, 4E, 4G) and 4Fe Fd_B^{ox} (peak B_{24}^o in Figure 5G). The pattern of tertiary NOEs in the 4Fe *Pf* Fds is very similar to that observed in the 3Fe *Pf* Fd (Gorst et al., 1995a).

prominent peaks are labeled B_{19}^{r}–B_{24}^{r} in Figure 3 and A_{19}^{o}–A_{24}^{o} in Figure 5, and their chemical shifts are listed in Table 3.

DISCUSSION

Sequence-Specific Assignment of Ligated Cys. The protons of individual Cys are, in large part, identified by their scalar connectivities, although the $C_\alpha H$ *vs* $C_\beta Hs$ are unambiguously identified only by quantitative analysis of the steady-state NOEs in conjunction with their relaxation times. The ligated Cys are located by identifying three distinct CH_2 fragments; the T_1s for the two $C_\beta Hs$ for each are qualitatively consistent with their relative proximity to the ligated iron (4.2 ± 0.1 and 3.3 ± 0.2 Å for $C_\beta H$ and $C_{\beta'}H$, respectively) and very similar among the $C_\beta Hs$ (or $C_{\beta'}Hs$) for the three Cys. The present study confirms our proposal (Gorst et al., 1995a) that the sequence identity of the hyperfine shifted and paramagnetically relaxed ligands in cubane cluster Fd can be determined by detection of "standard" backbone NOEs between the Cys and the adjacent residues that do not require assumptions about tertiary structure. In fact, the NOEs from cluster ligands to remote residues can be used to determine tertiary structure (Donaire et al., submitted). The observation of relatively weakly relaxed signals for the NHs for Cys I and IV and the $C_\alpha H$ for Cys III, but strongly relaxed signals for $C_\alpha Hs$ of Cys I and IV and the NH of Cys III in 4Fe *Pf* Fd in both cluster oxidation states, allows these assignments and directly confirms that the ligating geometry of the three Cys is similar to that observed in (and largely conserved among) the crystallographically characterized cubane Fds (as shown qualitatively in Figure 1) (Adman et al., 1976; Fukayama et al., 1988; Stout et al., 1989; Backes et al., 1991; Kissinger et al., 1991). Moreover, in the present *Pf* Fd, it was possible to apply this assignment scheme independently in Fd^{ox} and Fd^{red}. To date, the only assignments for ligated Cys signals in a reduced Fd have been achieved on the basis of saturation transfer from assigned signals in Fd^{ox} (see below) (Bertini et al., 1992, 1994; Donaire et al., 1994).

Identification of the Fourth Cluster Ligand. The location of three hyperfine shifted/relaxed CH_2 fragments with similar relaxation properties that can be uniquely traced to the three ligated Cys (ligands I, III, and IV) leaves unassigned a less strongly hyperfine shifted/relaxed CH_2 fragment of ligand II (in fact, a CH_2CH fragment in Fd_B^{red}). In the case of Fd_B^{red}, the observed hyperfine shifts of ~18 and 10 ppm for signals B_5^r and B_9^r of ligand II are too large[7] to arise from dipolar shifts. Preliminary 2D NMR results on *Pf* 4Fe Fd have shown that the overall folding topology is very similar in the four redox states of *Pf* 4Fe Fd (Gorst et al., 1995b) and very similar to that described in detail for *Pf* 3Fe Fd^{ox} (Teng et al., 1994). The cluster environment of the latter protein, in turn, was shown to be very similar to that in the *Dg* 3Fe Fd crystal structure (Kissinger et al., 1991). The size of the hyperfine shifts, the AMX spin topology, and the largely conserved cluster environments, which provide no other reasonable side chain as ligand, therefore lead us to eliminate a solvent based ligand (*i.e.*, H_2O or OH^-) and propose the logical assignment of Asp 14 as the fourth ligand (ligand II) in *Pf* $4Fe_B^{red}$.

More detailed assignment of other 4Fe cluster containing Fd in the oxidized state (Bertini et al., 1992, 1994; Donaire et al., 1994) has shown that, while several protons from noncoordinated residues are severely relaxed by the cluster proximity, none of the those signals exhibit significant hyperfine shifts, confirming a largely isotropic magnetic center. Thus the AMX spin topology, large contact shifts, and characteristic anti-Curie temperature dependence argue that the fourth ligand is Asp 14 in Fd_A^{ox} as well. The similar NMR spectral properties of Fd_B^{red} and Fd_A^{red} or Fd_A^{ox} and Fd_B^{ox} indicate that the coordination to the cluster of ligand II, moreover, is independent of the redox state of Cys 21, Cys 48. The T_1s for the two $C_\beta H$ peaks of Asp 14 (~22, 15 ms) are longer than that for $C_{\beta'}H$ (the proton closer to the iron) for each Cys in Fd_B^{red}, consistent with the expectation of a larger distance resulting from an additional intervening atom in the carboxylate *vs* cysteinate ligation. The narrower linewidth (observed in 1D NOEs in Figure 3I) for $C_\alpha H$ than $C_\beta Hs$ of Asp 14 in Fd_B^{red} is also consistent with an orientation of the ligated Asp 14 with its backbone (*i.e.*, $C_\alpha H$, NH) similar to that adopted by Cys II in structurally characterized Fds (see Figure 1), and observed by ^1H NMR in the related Cys (ligand II) *Tl* Fd (Donaire et al., 1994).

Electronic Structure of the Oxidized Cluster. The hyperfine shift patterns for all four ligands, Cys 11, 17, and 56 and Asp 14, are found to be essentially the same in Fd_A^{ox} and Fd_B^{ox}, and for the ligated Cys, very similar to those reported for a variety of 4Fe Fd^{ox} with only Cys ligation (Phillips & Poe, 1993; Luchinat & Ciurli, 1993; Cheng & Markley, 1995). The strong similarity in the hyperfine shift magnitude, together with the characteristic anti-Curie temperature dependence for the resonances for all four ligands (supporting information), strongly supports a $S = 0$ ground state with thermal population of the $S = 1$, 2 states that is comparable to that observed in Fds with complete Cys ligation. Hence the spin couplings among the four oxidation state-equivalent $Fe^{+2.5}$ in the cluster do not appear to be significantly different in a 3 Cys/Asp *vs* 4 Cys ligation scheme. This conclusion, however, could have been anticipated on the basis of earlier studies of model compounds that involved ligation of a cubane cluster by three thiolates and one carboxylate (Weigel & Holm, 1991). In fact, the contact shift observed for acetate (Asp model) *vs* methanthiolate (Cys model) is in the ratio ~0.4 in the $[Fe_4S_4]^{+2}$ model compound, which compares with the value of ~0.4 in *Pf* Fd_A^{ox} using the mean $C_\beta H$ shift.[2] (Note, this shift ratio also supports a ligated Asp to 4Fe Fd_A^{ox}.) Therefore, we conclude that the magnetic coupling and spin ground state in the oxidized cluster are not altered significantly by Asp *vs* Cys ligation and that the ^1H NMR spectra of an oxidized cluster will not identify a ligated Asp without detailed assignment of the hyperfine shifted resonances which may not be resolved from the diamagnetic envelope.

Electronic Structure of the Reduced Cluster. Much more surprisingly, the $C_\beta Hs$ for the ligated Cys in Fd_B^{red} and Fd_A^{red} exhibit both hyperfine shifts (5–50 ppm) and relaxation properties (T_1s 5–30 ms) which are remarkably similar to those for all reported cubane Fd^{red} with only Cys ligation and $S = {}^1/_2$ ground state (Bertini et al., 1992, 1994; Luchinat

[7] The equation for the dipolar shift: $(g_{\parallel}^2 - g_{\perp}^2)\beta^2[S(S+1)]/9kT[(3\cos^2\theta - 1)/R_{Fe}^3]$, with R_{Fe} ~4.5 estimated for T_1 ~22 ms of peak B_5^r, and known g values (Park et al., 1991), leads to a maximum dipolar shift of 3.7 ppm at the optimal orientation in the magnetic coordinate system (*i.e.*, $\theta = 0°$, $3\cos^2\theta - 1 = 2$). On the other hand, protons with T_1 ~3 ms have R_{Fe} ~3 Å, for which the maximal dipolar shift is ~12 ppm.

& Ciurli, 1993; Donaire et al., 1994). Even the temperature dependence for the various shifts is both Curie and anti-Curie (Figure 7), as found for more common 4Fe Fd^{red}. Since both the hyperfine shifts and relaxation are expected to increase with the spin multiplicity for any populated paramagnetic ground state (eqs 1 and 2), our qualitative conclusions are that the ^1H NMR spectrum of *Pf* Fd^{red} at ambient temperature in solution *fails to provide evidence to support a significant population of an* $S = {}^3/_2$ *ground state*. This is in contrast to low temperature EPR observations for 4Fe Fd_B^{red}, Fd_A^{red} where the $S = {}^3/_2$ ground state dominates (Conover et al., 1990a; Telser et al., 1995). The expected correlations between spin ground state and the ^1H NMR spectral properties indicated by eqs 1 and 2 for ligated Cys have been observed in the reduced *Cp* Fd for which the four labile sulfurs for each cluster were replaced with selenium (Gaillard et al., 1987). The EPR detected low temperature $S = {}^3/_2$ ground state translated at ambient temperature ^1H NMR spectra with much larger Cys $C_\beta H$ contact shift (100−150 ppm) and much broader lines than observed for reduced Fd with $S = {}^1/_2$ ground state. The contradictory NMR *vs* ESR evidence for the spin ground state for *Pf* Fd cannot be resolved at this time. More detailed study of the reduced protein by other spectroscopic methods is required.

It is noted, however, that while the ^1H NMR spectra of *Pf* Fd do not support a dominant $S = {}^3/_2$ ground state, several spectral features are more complex than those presented previously for other Fd with a $[Fe_4S_4]^{+1}$ cluster (Bertini et al., 1992, 1994; Donaire et al., 1994). The variable temperature data have shown that the C_βHs for four ligated Cys exhibit pairwise Curie and anti-Curie behavior which can be rationalized by the antiferromagnetic coupling between a valence-delocalized $2Fe^{+2.5}$ with $S = {}^9/_2$, and a $2Fe^{+2}$ with $S = 4$, respectively (Bertini et al., 1992). Ideally, the temperature dependence of ligated Cys $C_\beta H$ shifts could be used to model the spin coupling topology among the four irons. However, these demand that a single $\langle S_z \rangle_Q$ is observed by all protons on a ligand coordinated to iron-Q. Even the use of the angular part of eq 1 to estimate Cys orientation (Busse et al., 1991; Bertini et al., 1994) has implicit the assumption that the $\langle S_z \rangle_Q$ is the same for both protons. The variable temperature data for *Pf* Fd do not reflect such simple behavior (see Figure 7). In fact, one Cys (Cys 17) in Fd_B^{red} has its three protons exhibit Curie-like (B_6^r), anti-Curie (B_7^r), and essential temperature independenct (B_1^r) contact shifts (Figure 7B). This behavior is inconsistent with the simple eq 1 that demands that all protons for a given residue reflect the same temperature dependent $\langle S_z \rangle$ of the ligated iron. For Cys 11, the C_βHs (B_2^r, B_4^r in Figure 7B) exhibit anti-Curie, while the $C_\alpha H$ exhibits Curie-like behavior (not shown). The basis for the complex behavior in *Pf* Fd^{red} is not understood. However, it is noted that the variable temperature ^1H NMR behavior of Cys resonances has not been completely described for any reduced Fd. The present results suggest caution in interpreting the temperature dependence of ligated Cys C_βHs hyperfine shifts in terms of the relevant spin coupling parameters in the $[Fe_4S_4]^{+1}$ Fd cluster.

One ^1H NMR spectral property apparently unique to reduced *Pf* 4Fe Fd is that the number of hyperfine shifted nonexchangeable proton resonances exceeds the number of protons on the four identified ligands, dictating that some protons on nonligated residues experience dipolar shift. Our assignments identify 11 of the 12 nonlabile protons on the four ligated residues, leaving only the $C_\alpha H$ of Cys 56 unassigned. However, of the remaining three resolved hyperfine shifted peaks which have not been assigned, B_{10}, B_{26}, and B_{27} (see Table 1), only one could arise from a ligand (*i.e.*, the Cys 56 $C_\alpha H$), and hence at least two such signals must result from nonligated residues. Such resolved hyperfine shifted nonlabile proton signals that arise from nonligated residues are not observed in the assigned ^1H NMR spectra of reduced 4Fe *Cp*, *Ca*, or *Tl* Fds (Bertini et al., 1992, 1994; Donaire et al., 1994). The origins of the dipolar shifted proton signals remain obscure, but assignments are being pursued. It is noted, however, that these dipolar shifted signals exhibit very short T_1 (~3 ms), or as close to an iron as the closest Cys $C_\beta H$ (~3 Å), which allows modest dipolar shifts[7] even for small magnetic anisotropy. Whether this apparent magnetic anisotropy in 4Fe *Pf* Fd^{red} is an electronic consequence of Asp 14 ligation, or is a result of a significantly perturbed cluster structure relative to Fds with only Cys ligation, remains to be determined. The investigation on the Asp 14 to Cys 14 mutant is in progress.

Influence of Cys 21, Cys 48 Redox State on the Cluster Properties. The patterns of hyperfine shifts for the A (disulfide bond) or B (free thiols) forms for 4Fe *Pf* Fd are pairwise very similar in each of the cluster oxidation states, as shown by the data in Tables 1 and 2. In the oxidized cluster, the influence of the disulfide vs free thiol is negligible. The reduced cluster exhibits more differences in shift magnitude, although the patterns of shifts are maintained (Table 1, Figure 7). Perhaps the most intriguing observations are that the variable temperature slopes for selected resonances for a given residue differ between Fd_B^{red} and Fd_A^{red} (*i.e.*, Cys 56 $C_\beta H$ peak B_3^r exhibits Curie behavior in the former, while the same proton (A_3^r) exhibits anti-Curie behavior in the latter; also Cys 17 $C_\beta H$ exhibits a temperature independent shift in Fd_B^{red} (B_1^r) but strong Curie behavior in Fd_A^{red} (A_1^r) (Figure 7)). On the other hand, not only is there a close correlation between the A and B form for the assigned signals for the four cluster ligands, but the unassigned hyperfine shifted signals (at least some of which arise from noncoordinated residues) for Fd^{red} nonlabile (A_{10}, A_{26}, A_{27} *vs* B_{10}, B_{26}, B_{27}) and labile protons (a_8, a_{28} *vs* b_8, b_{28}) are also closely paired (see Table 2). A more detailed comparison of the A and B forms may become possible when a robust interpretive basis for the hyperfine shifts in the reduced cluster has been developed.

Possible Structural/Functional Consequences of Asp Ligation. The analysis of the hyperfine shifted ligand resonances indicates that the electronic properties of both oxidation states of the cluster in *Pf* Fd are similar to those from 4Fe Fd clusters with all Cys ligation. Perhaps the most distinctive ^1H NMR detected property of *Pf* 4Fe Fd relative to other NMR studied 4Fe Fd is the rate of electrons exchanged between the two cluster oxidation states. In all cases where such studies have been reported, there is observed strong saturation transfer between Fd^{ox} and Fd^{red} due to electron exchange. In fact, such saturation transfer to Fd^{ox} upon saturating signals Fd^{red} is so dominant as to seriously interfere with detecting NOEs within the Fd^{red} complex (Bertini et al., 1992, 1994; Donaire et al., 1994). The saturation factor for a peak B_i^o in Fd^{ox}, upon saturating peak B_i^r in Fd^{red}, is

given by (Sandström, 1982):

$$SF = \frac{T_1^{-1}(B_i^{o})}{k + T_1^{-1}(B_i^{o})} \quad (7)$$

where k is the rate of electron exchange. Qualitative comparison of *Pf* 4Fe Fd_B and *Tl* 4Fe Fd, which is also a hyperthermophilic protein but with a single cluster with complete Cys coordination, under similar solution conditions indicates that SF is over a factor of 10 smaller in *Pf* than *Tl* Fd (Donaire et al., 1994). Since the T_1s for the peaks in Fd^{ox} are comparable, this dictates that the electron self-exchange is ~10 times *slower* in *Pf* than in *Tl* Fd. The much slower electron exchange rate is the property that allows us to independently pursue the solution structures of Fd^{ox} and Fd^{red}.

A possible role for the Asp 14 in retarding electron exchange rates in *Pf* Fd is suggested by comparing the patterns of hyperfine shifts for C_βHs for the four ligands in the four redox states (Tables 1 and 2). Thus the relative δ_{hf} for the two C_βHs in the three Cys ligands remain qualitatively the same in the four redox states, which is consistent with similar Fe−S−C−H dihedral angles (*i.e.*, eq 3). The Asp C_βHs, however, reverse the relative δ_{hf} between oxidized and reduced clusters. This suggests that the Asp 14 ligand (and possibly adjacent residues) adopts a different orientation with cluster oxidation states. The longer side chain for Asp *vs* Cys would suggest that such local cluster oxidation state-sensitive "conformational" change is more likely for Asp than Cys. A second possible role for Asp 14 is that (in contrast to Cys) it could serve as either monodentate or bidentate ligand (Weigel & Holm, 1991), and its mode of coordination may be oxidation state-dependent. Either or both of these properties could serve to "gate" the electron exchange rate. A definitive test of this hypothesis is to characterize in a similar fashion the Asp 14 → Cys mutant, and such studies are in progress.

ACKNOWLEDGMENT

The authors are indebted to Dr. J. S. de Ropp for numerous valuable discussions.

SUPPORTING INFORMATION AVAILABLE

Five figures, showing ^1H NMR spectra of 4Fe Fd_B^{red} in ^1H_2O and ^2H_2O, MCOSY spectrum of 4Fe Fd_B^{red}, WEFT-NOESY spectrum of 4Fe Fd_B^{red}, WEFT-NOESY spectrum of 4Fe Fd_A^{ox}, and Curie plots for ligand protons for 4Fe Fd_A^{ox} and 4Fe Fd_B^{ox} (5 pages). Information for obtaining this material is provided on the masthead page.

REFERENCES

Adman, E. T., Sieker, L. C., & Jensen, L. H. (1976) *J. Biol. Cheml. 251*, 3801−3806.

Aono, S., Bryant, F. O., & Adams, M. W. W. (1989) *J. Bacteriol. 171*, 3433−3439.

Backes, G., Mino, Y., Loehr, T. M., Meyer, T. E., Cusanovich, M. A., Sweeney, W. V., Adman, E. T., & Sanders-Loehr, J. (1991) *J. Am. Chem. Soc. 113*, 2055−2064.

Bax, A. (1982) *Two Dimensional NMR in Liquids*, Reidel Publishing Co., Dordrecht, The Netherlands.

Bax, A., & Davis, D. G. (1985) *J. Magn. Reson. 65*, 355−360.

Beinert, H. (1990) *FASEB J.* 4, 2483−2491.

Beinert, H., & Kennedy, M. C. (1989) *Eur. J. Biochem. 186*, 5−15.

Bertini, I., Briganti, F., Luchinat, C., Messori, L., Monnanni, R., Scozzafava, A., & Vallini, G. (1992) *Eur. J. Biochem. 204*, 831−835.

Bertini, I., Capozzi, F., Luchinat, C., Piccioli, M., & Vila, A. J. (1994) *J. Am. Chem. Soc. 116*, 651−660.

Bovier-Lapierre, G., Bruschi, M., Bonicel, J., & Hatchikian, E. C. (1987) *Biochim. Biophys. Acta 913*, 20−26.

Brown, S. C., Weber, P. L., & Müller, L. (1988) *J. Magn. Reson. 77*, 166−169.

Busse, S. C., La Mar, G. N., & Howard, J. B. (1991) *J. Biol. Chem. 266*, 23714−23723.

Busse, S. C., La Mar, G. N., Yu, L. P., Howard, J. B., Smith, E. T., Zhou, Z. H.-, & Adams, M. W. W. (1992) *Biochemistry 31*, 11952−11962.

Cammack, R. (1992) *Adv. Inorg. Chem. 38*, 281−322.

Cammack, R., Dickson, D., & Johnson, C. (1977) in *Iron Sulfur Proteins* (Lovenberg, W., Ed.) pp 283−330, Academic Press, New York.

Chen, Z., de Ropp, J. S., Hernandez, G., & La Mar, G. N. (1994) *J. Am. Chem. Soc. 116*, 6841−6849.

Cheng, H., & Markley, J. L. (1995) *Annu. Rev. Biophys. Biomol. Struct. 24*, 209−237.

Conover, R. C., Kowal, A. T., Fu, W., Park, J.-B., Aono, S., Adams, M. W. W., & Johnson, M. K. (1990a) *J. Biol. Chem. 265*, 8533−8541.

Conover, R. C., Park, J.-B., Adams, M. W. W., & Johnson, M. K. (1990b) *J. Am. Chem. Soc. 112*, 4562−4564.

Conover, R. C., Park, J.-B., Adams, M. W. W., & Johnson, M. K. (1991) *J. Am. Chem. Soc. 113*, 2799−2800.

Donaire, A., Gorst, C. M., Zhou, Z.-H., Adams. M. W. W., & La Mar, G. N. (1994) *J. Am. Chem. Soc. 116*, 6841−6849.

Donaire, A., Zhou, Z.-H., Adams, M. W. W., & La Mar, G. N. (1995) *J. Biomol. NMR* (submitted for publication).

Emptage, H. (1988) in *Metal Clusters in Proteins* (Que, L., Jr., Ed.) Vol. 372, pp 343−371, American Chemical Society, Washington, DC.

Flint, D. H., Emptage, M. H., Finnegan, M. G., Fu, W., & Johnson, M. K. (1993) *J. Biol. Chem. 268*, 14732−14742.

Fu, W., Telser, J., Hoffman, B. M., Smith, E. T., Adams, M. W. W., & Johnson, M. K. (1994) *J. Am. Chem. Soc. 116*, 5722−5729.

Fukuyama, K., Nagahara, Y., Tsukihara, T., Katsube, Y., Hase, T., & Matsubara, H. (1988) *J. Mol. Biol. 199*, 183−193.

Gaillard, J., Moulis, J.-M., & Meyer, J. (1987) *Inorg. Chem. 26*, 320−324.

Gaillard, J., Albrand, J.-P., Moulis, J.-M., & Wemmer, D. E. (1992) *Biochemistry 31*, 5632−5639.

George, S. J., Armstrong, F. A., Hatchikian, E. C., & Thomson, A. J. (1989) *Biochem. J. 264*, 275−284.

Gorst, C. M., Yeh, Y., Teng, Q., Calzolai, L., Zhou, Z., Adams, M. W. W., & La Mar, G. N. (1995a) *Biochemistry 34*, 600−610.

Gorst, C. M., Zhou, Z., Kesen, M. Q., Teng, Q., Howard, J. B., Adams, M. W. W., & La Mar, G. N. (1995b) *Biochemistry 34*, 8788−8795.

Hofmeister, A. E. M., Albracht, S. P. J., & Buckel, W. (1994) *FEBS Lett. 351*, 416−418.

Howard, J. B., & Rees, D. C. (1991) *Adv. Protein Chem. 42*, 199−281.

Inubushi, T., & Becker, G. D. (1983) *J. Magn. Reson. 51*, 128−133.

Iwasaki, T., Wakagi, T., Isogai, Y., Tanaka, T., Iizuka, T., & Oshima, T. (1994) *J. Biol. Chem. 269*, 29444−29450.

Johnson, M. K. (1994) in *Encyclopedia of Inorganic Chemistry* (King, R. B., Ed.) pp 1896−1915, John Wiley, New York.

Kennedy, M. C., & Stout, C. D. (1992) *Adv. Inorg. Chem. 38*, 323−339.

Kissinger, C. R., Sieker, L. C., Adman, E. T., & Jensen, L. H. (1991) *J. Mol. Biol. 219*, 693−715.

La Mar, G. N., & de Ropp, J. S. (1993) in *Biological Magnetic Resonance* (Berliner, L. J., & Reuben, J., Eds.) Vol. 12, pp 1−78, Plenum Press, New York.

Lauble, H., Kennedy, M. C., Beinert, H., & Stout, C. D. (1994) *J. Mol. Biol. 237*, 437−451.

Luchinat, C., & Ciurli, C. (1993) *Biol. Magn. Reson. 12*, 357−420.

Macedo, A. L., Moura, I., Surerus, K. K., Papaefthymiou, V., Luis, M. Y., LeGall, J., & Munch, E. (1994) *J. Biol. Chem. 269*, 8052−8058.

Matsubara, H., & Saeki, K. (1992) *Adv. Inorg. Chem. 38*, 223−280.

Minami, Y., Wakabayashi, S., Wada, K., Matsubara, H., Kersher, L., & Oesterhelt, D. (1983) *J. Biochem. 97*, 745−753.

Moura, J. J. G., Macedo, A. L., & Palma, P. N. (1994) *Methods Enzymol. 243*, 165−188.

Neuhaus, D., & Williamson, M. (1989) *The Nuclear Overhauser Effect in Structural and Conformational Analysis*, VCH Publications, New York.

Okawara, N., Ogata, M., Yagi, T., Wakabayashi, S., & Matsubara, H. (1988) *J. Biochem. 104*, 196−199.

O'Keefe, D. P., Gibson, K. J., Emptage, M. H., Lenstra, R., Romesser, J. A., Little, P. J., & Omer, C. A. (1991) *Biochemistry 30*, 447−455.

Park, J.-B., Fan, C., Hoffman, B. M., & Adams, M. W. W. (1991) *J. Biol. Chem. 266*, 19351−19356.

Phillips, W. D., & Poe, M. (1973) in *Iron Sulfur Proteins* (Lovenberg, W., Ed.) Vol. II, pp 255−285, Academic Press, New York.

Sandström, J. (1982) *Dynamic NMR Spectroscopy*, Academic Press, New York.

Smart, L. B., Warren, P. V., Golbeck, J. H., & Mcintosh, L. (1992) *Proc. Natl. Acad. Sci. U.S.A. 90*, 1132−1136.

Srivastava, K. K. P., Surerus, K. K., Conover, R. C., Johnson, M. K., Park, J.-B., Adams, M. W. W., & Münck, E. (1993) *Inorg. Chem. 32*, 927−936.

Stout, C. D. (1989) *J. Biol. Chem. 263*, 9256−9266.

Telser, J., Smith, E. T., Adams, M. W. W., Conover, R. C., Johnson, M. K., & Hoffman, B. M. (1995) *J. Am. Chem. Soc.* (in press).

Teng, Q., Zhou, Z. H., Smith, E. T., Busse, S. C., Howard, J. B., Adams, M. W. W., & La Mar, G. N. (1994) *Biochemistry 33*, 6316−6326.

Wakabayashi, S., Fujimoto, N., Wada, K., Matsubara, H., Kerscher, L., & Oesterhelt, D. (1983) *FEBS Lett. 162*, 21−24.

Warren, P. V., Smart, L. B., Mcintosh, L., & Golbeck, J. H. (1992) *Biochemistry 32*, 4411−4419.

Weigel, J. A., & Holm, R. H. (1991) *J. Am. Chem. Soc. 113*, 4184−4191.

Wüthrich, K. (1986) *NMR of Proteins and Nucleic Acids*, Wiley, New York.

BI9510486